Metal-Centered Photoluminescence as a Tool for Detecting Phase Transitions in Eu^{III}- and Tb^{III}-Containing Metallomesogens

Stéphane Suárez,† Daniel Imbert,† Frédéric Gumy,† Claude Piguet,‡ and Jean-Claude G. Bünzli*,†

Laboratory of Lanthanide Supramolecular Chemistry, Swiss Federal Institute of Technology Lausanne, BCH 1402, 1015 Lausanne, Switzerland, and Department of Inorganic, Analytical and Applied Chemistry, University of Geneva, 30 quai E. Ansermet, 1211 Geneva 4, Switzerland

Received February 17, 2004. Revised Manuscript Received June 9, 2004

The non-mesogenic ligand **L¹**, derived from a 1,7-diaza-18-crown ether, forms mesogenic complexes with Eu^{III} and Tb^{III} nitrates, $Eu(NO_3)_3$**L¹**·0.25 H_2O (**EuL¹**) and $Tb(NO_3)_3$**L¹**·1 THF (**TbL¹**). Thermal analyses and polarized light microscopy data indicate the formation of a liquid-crystalline phase at 86 (Eu) and 81 °C (Tb), while isotropization occurs around 198−200 °C, immediately followed by decomposition. In the case of Eu^{III}, the mesogenic phase is unambiguously identified as being a hexagonal columnar mesophase by SAXD. According to a detailed luminescence study, the crystalline form of **EuL¹** features two different metal ion environments: (i) a C_2-symmetrical site without coordinated water molecule (population: 79 ± 6%) and (ii) a low-symmetry site with one water molecule coordinated onto the metal ion (population: 21 ± 6%). For **EuL¹**, the variation of both the relative intensity of the $^5D_0 \rightarrow {}^7F_2$ transition, $\ln(I_T/I_{295})$, and of the $Eu(^5D_0)$ lifetime, $\ln(\tau_T/\tau_{295})$, over the Cr−Col_h transition have a S-shape dependence versus $1/T$, allowing a precise determination of the transition temperature. In the case of the luminescence intensity, corrections for the expected decrease versus increasing temperature (determined on a reference compound **EuL²** with **L²** devoid of mesogenic side chains) and for the refractive index change over the transition still leave a sigmoid dependence, pointing to a genuine effect generated by the phase transition. Consequently, luminescence intensity and lifetime switching can be used to signal Cr−LC transitions in Eu-containing mesogenic compounds. A similar effect is observed for **TbL¹**, as far as the intensity of the $^5D_4 \rightarrow {}^7F_5$ transition is concerned.

Introduction

Lanthanide-containing liquid crystals are attracting a great deal of research efforts[1] because incorporation of 4f ions into mesogenic phases allows the tailoring of devices taking advantage of the unique optical and magnetic properties of these ions. One specific aspect consists of the preparation of luminescent liquid crystals for LCDs, eliminating the need for photoluminescent sheets acting as filters and which considerably reduce the emission efficiency of the devices. Indeed, phosphors used in lighting devices or in various displays are based on lanthanide-containing trichromatic materials emitting narrow bands in the three basic colors [blue (Eu^{II}), green (Tb^{III}), and red (Eu^{III})][2] because these ions have emission characteristics matching well the physiological response of the eye. Moreover, lanthanide-doped mesogenic materials have also a definite advantage over organic-based luminescent liquid crystals since the latter often display a broad-band, usually blue, emission that is of limited practical use.

There are basically two strategies for designing lanthanide-containing liquid crystals. One is to synthesize mesogenic or pro-mesogenic ligands leading to mesogenic lanthanide complexes. Initially, it was thought that introducing bulky spherical Ln^{III} ions in potentially mesogenic compounds could disrupt the required order to produce mesophases. However, it turned out that many lanthanide-containing systems are in fact amenable to form liquid crystalline phases.[1] The first such compound, bis(octaalkyloxyphthalocyaninato)lutetium, was reported by Piechocki in 1985.[3] Other properties of the Ln^{III} ions can be helpful in liquid crystals, for instance, their varying size along the series which can be used to fine-tune the properties of the mesomorphic phases.[4] Such a strategy sometimes involves a large synthetic effort to produce ligands fitted with the adequate pro-mesogenic chains, and some authors have explored another route, which appears simpler. It consists of doping lanthanide salts or complexes, for instance, the highly luminescent β-diketonates, in known

* Corresponding author e-mail: jean-claude.bunzli@epfl.ch.
† Swiss Federal Institute of Technology Lausanne.
‡ University of Geneva.

(1) Binnemans, K.; Görller-Walrand, C. *Chem. Rev.* **2002**, *102*, 2303.
(2) Ozawa, L.; Itoh, M. *Chem. Rev.* **2003**, *103*, 3835.
(3) Piechocki, C.; Simon, J.; André, J. J.; Guillon, D.; Petit, P.; Skoulios, A.; Weber, P. *Chem. Phys. Lett.* **1985**, *122*, 124.
(4) Terazzi, E.; Benech, J.-M.; Rivera, J.-P.; Bernardinelli, G.; Donnio, B.; Guillon, D.; Piguet, C. *J. Chem. Soc., Dalton Trans.* **2003**, 769.

10.1021/cm049754t CCC: $27.50
Published on Web 07/31/2004

cholesteric[5,6] and nematic[7,8] phases as well as in a smectic ionic liquid.[9]

Conventional techniques to monitor phase transitions in mesogenic materials rely usually on thermal analyses, polarized light microscopy, and small-angle X-ray diffraction. The latter two techniques are required when the exact nature of the mesophase has to be unraveled. On the other hand, when an appraisal of the temperature transition only is needed, differential thermal analysis (DTA) or differential scanning calorimetry (DSC) is sufficient but subject to hysteresis effects depending on the heating rate. Another, relatively unexplored approach is to resort to changes in luminescence properties. Indeed, specific luminescence intensity and excited-state lifetime are expected for each phase since the lattice parameters, site symmetry, and long-range order will alter over the phase transition. These changes are expected to be more pronounced for first-order transitions and will result in discontinuities in the luminescence properties. Until now, such effects have been taken advantage of for a rapid assessment of melting points[10] or of some inorganic materials, in particular with respect to assessing their purity.[11] Since several lanthanide ions display metal-centered luminescence properties (e.g., Eu^{III} and Tb^{III}), we consequently explore here the possibility of determining the temperature of the crystalline to liquid crystalline (Cr-LC) phase transitions by monitoring these properties. The Eu^{III} ion is a convenient analytical and structural probe[12−14] due to both its ground state ($^7F_0$) and most luminescent excited state ($^5D_0$) having a J quantum number equal to zero. To our knowledge, only few papers have exploited the Eu^{III} ion to probe liquid crystalline phases. For instance, the degree of disorder around the metal ion in metastable liquid crystals based on europium laurate has been established at very low temperature,[15] and second-rank crystal-field parameters have been worked out through analysis of the $^5D_0 \rightarrow {}^7F_1$ transition in order to assess the magnetic anisotropy of europium-containing metallomesogens.[16]

In this paper, we build on our initial communication reporting how luminescence intensity and excited-state lifetime can signal Cr−LC transitions in a Eu^{III} complex built from a substituted diaza-18-crown-6 macrocyclic ligand.[17] First, we investigate in details the photophysical properties of the crystalline phase of the Eu^{III} complex. We then analyze the possible contributions to the spike in the luminescence intensity (S-shape curve) over the Cr−LC transition temperature in terms of temperature-dependent nonradiative de-excitations processes, refractive index variation, and intrinsic contribution from the phase transition. Finally, we extend the method to the Tb^{III} complex (see Chart 1).

Chart 1

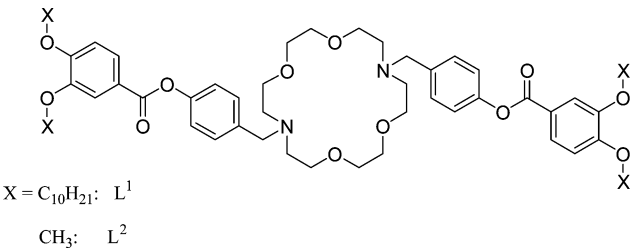

Table 1. Differential Scanning Calorimetric Data for the Ligands and Their Ln^{III} Complexes

compd	transition[a]	T (°C)	ΔH (kJ·mol^{-1})	ΔS (J·mol^{-1}·K^{-1})
L^1	Cr−I	85	100	279
EuL^1	Cr−Col_h[b]	86	20	56
	Col_h−I[c]	200		
TbL^1	Cr−Col_h[b]	81	11	32
	Col_h−I[c]	195		
L^2	Cr−I	166	99	226
EuL^2	Cr−I[c]	159	15	35

[a] Cr = crystalline phase, I = isotropization, Col_h = hexagonal columnar phase. [b] Determined by X-ray diffraction. [c] Isotropization followed by decomposition.

Results and Discussion

Mesogenic Properties. Phase transitions for ligands **L^1**, **L^2**, and their Ln^{III} complexes [$Eu(NO_3)_3L^1 \cdot 0.25H_2O$ (**EuL^1**), $Tb(NO_3)_3L^1 \cdot 1THF$ (**TbL^1**), and $Eu(NO_3)_3L^2 \cdot 1.5H_2O$ (**EuL^2**)] have been analyzed by thermogravimetry, differential scanning calorimetry, and polarized light microscopy (PLM). Relevant data including the associated enthalpy and entropy values are summarized in Table 1. The free ligands display a standard non-mesogenic behavior with isotropization occurring at 85 (L^1) and 166 °C (L^2). This large difference being a consequence of the long alkyl substituents on L^1, which increases the entropic contribution to the melting process.[18] The reference complex **EuL^2** exhibits a similar behavior, as expected. On the other hand, the Ln^{III} complexes with **L^1** present an interesting mesogenic behavior. During the first heating cycle, the two investigated compounds lose their solvation molecules (water or THF), so that data in Table 1 refer to the second heating cycle. Indeed, mesomorphic properties of solvated complexes usually differ largely from those of nonsolvated species or may even be inhibited as described in the case of bowl-shaped tungsten complexes with derivatized calix[4]arenes.[19] For **EuL^1**, TG curves

(5) Yu, L. J.; Labes, M. M. *Appl. Phys. Lett.* **1977**, *31*, 719.
(6) Boyaval, J.; Li, C.; Hapiot, F.; Warenghem, M.; Isaert, N.; Guyot, Y.; Boulon, G.; Carette, P. *Mol. Cryst. Liq. Cryst.* **2001**, *359*, 337.
(7) Binnemans, K.; Moors, D. *J. Mater. Chem.* **2002**, *12*, 3374.
(8) Van Deun, R.; Moors, D.; De Fre, B.; Binnemans, K. *J. Mater. Chem.* **2003**, *13*, 1520.
(9) Guillet, E.; Imbert, D.; Scopelliti, R.; Bünzli, J.-C. G. Submitted for publication.
(10) Blackwell, G. R.; Busby, R. E. *J. Sci. Instrum.* **1965**, *42*, 167.
(11) Townsend, P. D.; Maghrabi, M.; Yang, B. *Nucl. Instr. Methods Phys. Res. B* **2002**, *191*, 767.
(12) Bünzli, J.-C. G. In *Lanthanide Probes in Life, Chemical and Earth Sciences. Theory and Practice*; Bünzli, J.-C. G., Choppin, G. R., Eds.; Elsevier Science: Amsterdam, 1989, Chapter 7.
(13) Bünzli, J.-C. G.; Piguet, C. In *Encyclopedia of Materials: Science and Technology*; Buschow, K. H. J., Cahn, R. W., Flemings, M. C., Ilschner, B., Kramer, E. J., Mahajan, S., Eds.; Elsevier Science: Oxford, 2001; Vol. 10, Chapter 1.10.4.
(14) Bünzli, J.-C. G. In *Spectroscopic Properties of Rare Earths in Optical Materials*; Liu, G. K., Jacquier, B., Eds.; Springer-Verlag: Berlin, 2004, Chapter 11 (in press).
(15) Corkery, R. W.; Martin, J. P. D. *J. Lumin.* **1999**, *82*, 1.
(16) Binnemans, K.; Malykhina, L.; Mironov, V. S.; Haase, W.; Driesen, K.; Van Deun, R.; Fluyt, L.; Gorller-Walrand, C.; Galyametdinov, Y. G. *ChemPhysChem* **2001**, *2*, 680.
(17) Suárez, S.; Mamula, O.; Imbert, D.; Piguet, C.; Bünzli, J.-C. G. *Chem. Commun.* **2003**, 1226.
(18) Nozary, H.; Piguet, C.; Rivera, J.-P.; Tissot, P.; Bernardinelli, G.; Vulliermet, N.; Weber, J.; Bünzli, J.-C. G. *Inorg. Chem.* **2000**, *39*, 5286.
(19) Xu Bing; Swager, T. M. *J. Am. Chem. Soc.* **1993**, *115*, 1159.

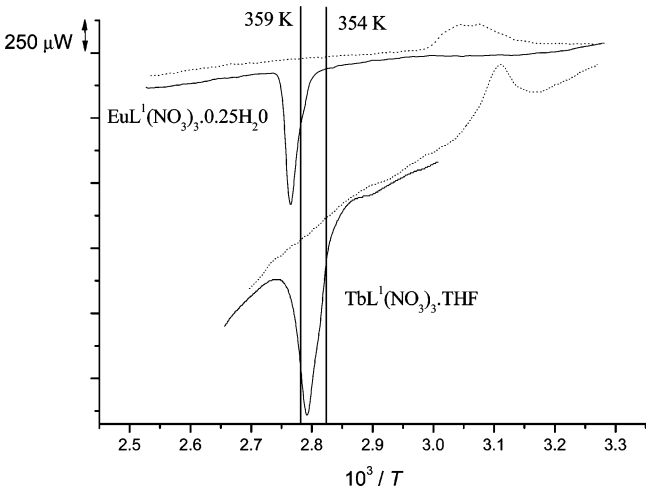

Figure 1. DSC traces of the LnL^1 complexes (Ln = Tb, Eu) at 5 °C·min^{-1} from 25 to 130 °C (—) and from 130 to 25 °C (···).

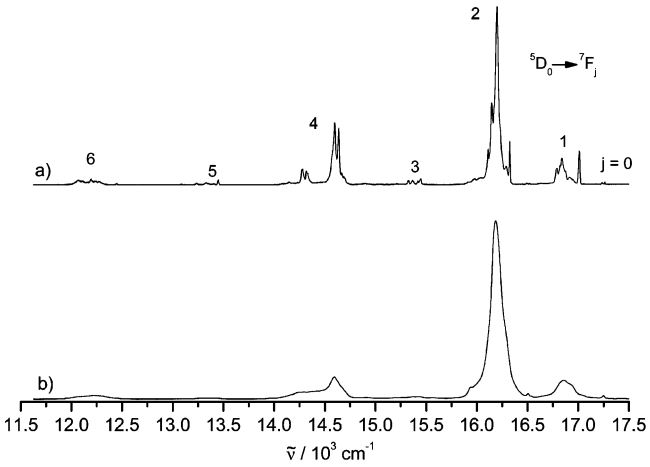

Figure 2. High-resolution emission spectra of a solid-state sample of **EuL¹** recorded at (a) 10 and (b) 295 K, $\tilde{\nu}_{ex}$ = 24 468 cm^{-1}.

show progressive weight loss up to the melting point at 199 °C corresponding to the loss of one-fourth water molecule per formula weight. During the first heating cycle, the DSC curve points to a Cr−LC transition at 87 °C with a second exothermic and irreversible transformation at 124 °C, which could correspond to a partial disorganization of the mesogenic phase. Isotropization around 198−200 °C is immediately followed by decomposition of the sample. Provided the sample is not heated above 170 °C, reversible thermograms are obtained over many heating−cooling cycles, which lack the 124 °C event, and with a hysteresis of about 25 °C for the Cr→LC transition, under a heating rate of 5 °C·min^{-1} (Figure 1). The metastable form obtained during the first heating cycle is a commonly observed feature, and one proposed explanation is that it enables the formation of a thermodynamically more stable mesomorphic phase.[20] The liquid-crystalline phase occurring between 85 and 198 °C has been further characterized by polarized light microscopy, which clearly confirmed that the endothermic peak at 86 °C corresponds to a first-order Cr→LC transition. Finally, a preliminary X-ray investigation at small angles revealed a Bragg's fine structure characteristic of a lamellar mesophase with a periodicity around 42−45 Å appearing during the first heating cycle and then, upon cooling, a well-characterized and reversible columnar hexagonal phase (Col_h, with the observation of three fine reflections by X-ray diffraction corresponding to the squared spacing ratios $h^2 + k^2 + hk = 1, 3, 4$, and the indexation $(hk) = (10), (11), (20)$).[21] The behavior of **TbL¹**, as unraveled by thermal (Figure 1) and optical methods, is very similar with a first-order transition Cr→LC at 81 °C; the mesophase persists up to isotropization at 195 °C, immediately followed by decomposition.

Multi-Center Luminescence of the Eu^{III} and Tb^{III} Complexes. In THF, the ligands display three absorption bands centered at 45 300, 37 500, and 34 000 cm^{-1} (Table S1 in Supporting Information). UV excitation in these absorption bands yields no emission spectrum at room temperature. However, at 77 K, a solid-state sample of **L¹** presents two emission bands assigned to emission from the $^1\pi\pi^*$ and $^3\pi\pi^*$ states, with maxima at 30 670 and 20 760 cm^{-1}, respectively. The latter is weak and only observed in time-resolved mode, pointing to an inefficient intersystem crossing, which can be explained by the large energy gap between the 0-phonon transitions of the two states ($\Delta E(^1\pi\pi^* - {}^3\pi\pi^*) > 9000$ cm^{-1}).[22] For ligand **L²**, no singlet state emission is detected, even at 77 K, but only a weak emission from the $^3\pi\pi^*$ state at 77 K. The absence of luminescence at ambient temperature for both ligands reveals significant nonradiative deactivation processes in these systems. A red shift (≈1000 cm^{-1}) of the singlet state is observed after complexation of ligand **L¹** with Eu^{III} ($E(^1\pi\pi^*)$ = 29 590 cm^{-1}) and Tb^{III} (29 410 cm^{-1}), while no emission from the singlet state of complexed ligand **L²** occurs. Time-resolved luminescence spectra of the complexes reveal complete disappearance of the triplet state emission, along with a strong luminescence characteristic of the metal-centered emission, pointing to a fast energy transfer from the $^3\pi\pi^*$ state to the Eu($^5D_0$) or Tb($^5D_4$) excited levels. Sizable emission from the terbium complex was expected, since the energy gap $\Delta E(^3\pi\pi^* - {}^5D_4)$ = 2530 cm^{-1} is in good agreement with what is generally considered as being a favorable situation for ligand-to-metal energy transfer.[14] We also observe a metal-centered emission for **EuL¹** and **EuL²**, for which $\Delta E(^3\pi\pi^* - {}^5D_0)$ is equal to 6300 and 5300 cm^{-1}, respectively. In the following, we first take advantage of Eu^{III} as a structural luminescent stain to probe the structure of **EuL¹** since no crystal amenable to X-ray investigation could be grown for this compound, nor for **EuL²**. We then demonstrate how the luminescence properties of both Eu^{III} and Tb^{III} can be used to monitor the phase transitions.

High-Resolution Luminescence of LnL^1. Irradiation through the ligand-centered levels of **EuL¹** at low (10 K) and room temperature (295 K) provides the spectra reported in Figure 2. Relative, corrected, and integrated intensities of the $^5D_0 \rightarrow {}^7F_J$ transitions are

(20) Jongen, L.; Goderis, B.; Dolbnya, I.; Binnemans, K. *Chem. Mater.* **2003**, *15*, 212.

(21) Suárez, S.; Mamula, O.; Imbert, D.; Donnio, B.; Guillon, D.; Scopelliti, R.; Piguet, C.; Bünzli, J.-C. G. Unpublished results.

(22) Steemers, F. J.; Verboom, W.; Reinhoudt, D. N.; Vandertol, E. B.; Verhoeven, J. W. *J. Am. Chem. Soc.* **1995**, *117*, 9408.

Table 2. Energy (cm^{-1}) of Identified Crystal Field Sublevels of Eu(^7F_J) Manifold ($J = 1-4$) in EuL[1] As Determined from Excitation and Emission Spectra in Solid State at 10 K[a]

level	site I[b]	site II[c]	level	site I[b]	site II[c]
$^7F_0$	0		$^7F_3$	1820	
$^7F_1$	258			1849	
	291[d]	322		1899	1874
		363		1938	
	422				
	448	415	$^7F_4$	2581[d]	2546
	477[d]			2597[d]	2572
				2629	
$^7F_2$	941			2670	2661
	958[d]	948		2943	
	1012[d]			2982	
	1074	1033	$^5D_0$	17266	17242
	1119	1064			
	1154	1079[d]			
	1221[d]				
	1281[d]				

[a] $^7F_0$ is taken as the origin. [b] $\tilde{\nu}_{ex} = 17\,266\ cm^{-1}$. [c] $\tilde{\nu}_{ex} = 17\,242\ cm^{-1}$. [d] Vibronic transition

reported in Table S2 (Supporting Information), while electronic sublevels of the ^7F_J ($J = 1-6$) manifold are listed in Table 2. The emission spectrum is dominated by transitions to the $^7F_2$ sublevels, in line with a low symmetry around the Eu^{III} ion.[12,14]

At 295 K, the $^5D_0 \rightarrow {}^7F_0$ transition is observed as a very weak and slightly asymmetrical broad band (full width at half-height, fwhh = 17 cm^{-1}) with a maximum at 17 278 cm^{-1}. At 10 K, three components are detected at 17 266 cm^{-1} (site I, fwhh = 7 cm^{-1}, from multi-peak fitting, see Figure S1 in Supporting Information), at 17 244 cm^{-1} (site IIa, fwhh = 10 cm^{-1}) and 17 235 cm^{-1} (site IIb, fwhh = 18 cm^{-1}). Since excitation on either one of the latter two components yields very similar emission spectra, we interpret these data as if there were only two different Eu(III) coordination sites and label the two components of the 0−0 transition arising at lower energy as site II.

To confirm this interpretation, we have resorted to high-resolution laser-excited excitation spectroscopy of the $^5D_0 \leftarrow {}^7F_0$ transition. The excitation profile of this transition, obtained by monitoring several components of the $^5D_0 \rightarrow {}^7F_{1,2}$ transitions (Figure 3, Table S3 in Supporting Information), indeed reflects the presence of (i) a symmetrical band labeled I at 17 266 cm^{-1} with an additional weak component at 17 282 cm^{-1} on the high energy side and (ii) a multicomponent feature labeled II with two main bands at 17 242 cm^{-1} (IIa) and 17 249 cm^{-1} (IIb). Increasing the temperature to 295 K results in a single broad band centered at 17 278 cm^{-1} corresponding to site I. The temperature dependence of the $^5D_0 \leftarrow {}^7F_0$ excitation spectra is depicted in Figure S2 (Supporting Information).

Selective laser excitation of these 0−0 transitions produces the emission spectra reported in Figures S3 and S4 (Supporting Information). Excitation at 17 242 (IIa) and 17 250 cm^{-1} (IIb) yields two very similar emission spectra. There are three transitions to the $^7F_1$ sublevels, which are almost equally spaced ($\Delta E = 41$ and 52 cm^{-1}), with similar intensity and with a total splitting of 93 cm^{-1} (Table 2). This, together with the fact that the $^5D_0 \rightarrow {}^7F_2$ transition largely dominates the spectrum, points to metal ion sites with low symmetry (C_2, C_s, C_1). The minute differences between the emission spectra IIa and IIb may reflect the presence of slightly different conformations[23,24] induced by intermolecular interactions.

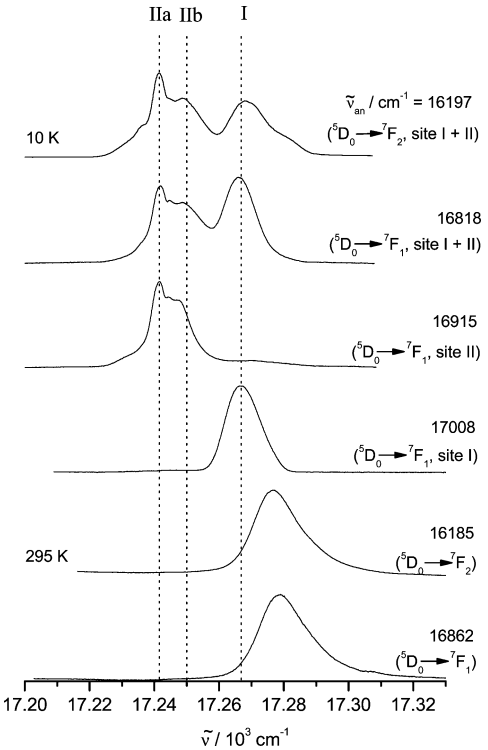

Figure 3. Excitation spectra in the range of the $^5D_0 \leftarrow {}^7F_0$ transition measured at 10 and 295 K for a solid-state sample of **EuL[1]**, upon monitoring the Eu($^5D_0 \rightarrow {}^7F_{1,2}$) transitions.

Some of the transitions in the emission spectrum obtained upon excitation at 17 266 cm^{-1} (site I, low symmetry) display more than ($2J + 1$) components, so that we have to find out whether energy transfer between sites I and II takes place. Focusing our attention on the $^5D_0 \rightarrow {}^7F_1$ transition (Figure S4 in Supporting Information), one clearly sees that no energy transfer occurs between the metal sites, since no component of the emission of II is seen in the spectrum obtained by selective excitation of site I (in particular, see component at 17 008 cm^{-1}). A similar situation prevails for the transitions to $^7F_2$, and $^7F_4$, so that one may conclude that no energy transfer occurs from site I to site II and that supplementary bands have a vibronic origin. Indeed, a correlation between the vibrational and luminescence spectra in the energy range of the transitions to $^7F_1$ and $^7F_2$ (Figures S5 in Supporting Information) shows following components having a vibronic origin: 291, 477, 958, 1012, 1221, and 1281 cm^{-1}. To better assess the site symmetry of site I, we have compared its emission spectrum to the one previously reported at 77 K for the C_2-symmetrical $[Eu(NO_3)_2Me_2\text{-}(2,2)]^+$ cationic species present in the 4:3 complex between europium nitrate and the diaza crown ether $Me_2(2,2)$.[24] Both spectra are very similar; therefore, we propose a C_2 symmetry for site I of the **EuL[1]** complex.

A population analysis based on the $^5D_0 \rightarrow {}^7F_1$ transition, the absolute intensity of which is in principle

(23) Bünzli, J.-C. G.; Pradervand, G.-O. *J. Chem. Phys.* **1986**, *85*, 2489.
(24) Nicolo, F.; Plancherel, D.; Chapuis, G.; Bünzli, J.-C. G. *Inorg. Chem.* **1988**, *27*, 3518.

independent of the site symmetry and chemical environment,[25] reveals that the emission from site I represents 79% ± 6 of the total emission. Since thermal and elemental analyses have shown **EuL¹** containing 0.25 water molecules per Eu^{III} ion, we assign sites II to a hydrated species. This hypothesis is consistent with the fact that, upon increasing the temperature, the corresponding $^5D_0 \leftarrow ^7F_0$ component becomes broader and eventually vanishes at 295 K (Figure S2 in Supporting Information) due to a larger contribution from vibronic components and possibly to a phase transition. Since the investigated compound bears a long and flexible chain on the nitrogen atoms instead of methyl groups, one indeed expects a larger vibrational contribution to the nonradiative deactivation. Therefore, at room temperature, only the component assigned to site I is visible, with a total energy shift from 10 to 295 K corresponding to the phenomenological dependence of 1 cm^{-1}/24 K.[12] The lifetime of the $Eu(^5D_0)$ level, which is highly sensitive to the presence of water in the inner coordination sphere, amounts to 1.08 ± 0.03 ms and 0.76 ± 0.03 ms at 10 and 295 K, respectively, upon direct excitation to site I and to 0.51± 0.03 ms for site II (Table S4 in Supporting Information). Comparing again these values with data on $[Eu(NO_3)_2Me_2(2,2)]_3Eu(NO_3)_6$,[24] we note that lifetimes of 1.06 ± 0.05 and 0.77 ± 0.02 ms have been reported at 77 and 295 K, respectively, for the cationic species which, according to the X-ray study, does not contain any water molecule, neither in the inner coordination sphere nor in the outer one. Our data are therefore consistent with the presence of one site (I) having the larger population and without coordinated water molecule. The site with the smaller lifetime and a population of 21 ± 6% would then correspond to a monohydrated chemical environment. The latter assumption is consistent with the chemical analysis of **EuL¹** and with the number of coordinated water molecules q calculated from the empirical eq 1:

$$q = A_{Ln}[\tau^{-1}(H_2O) - \tau^{-1}(D_2O)] \qquad (1)$$

in which A_{Ln} is 1.05 for Eu^{III} and $\tau^{-1}(H_2O)$ and $\tau^{-1}(D_2O)$ are the reciprocal of the observed lifetimes (ms^{-1}) in water and deuterated water, respectively.[26] Approximating $\tau(D_2O)$ as equal to the lifetime of site I at 10 K, we find q = 1.1, in good agreement with the above reasoning. Summarizing, analytical, thermal, and luminescence data point to the **EuL¹** sample analyzed in this study featuring two different metal ion sites: site I, with C_2 symmetry, without coordinated water molecule, and with a population of 3/4; and a low-symmetry site II, somewhat inhomogeneous, with one coordinated water molecule and a population of 1/4.

Luminescence data for **TbL¹** are less informative (Figure S6 in Supporting Information); the emission spectrum is dominated by the transition to the $^7F_5$ level and the $Tb(^5D_4)$ lifetime is relatively short (1.05−1.19 ms), although consistent with no coordinated water molecule[27] and temperature independent (Table S5 in Supporting Information).

Energy Migration Processes in EuL¹. Generally speaking, the rate of deactivation of the $Eu(^5D_0)$ excited state may be written as follows:

$$k = k_r + k_{nr} + k_{nr}(\text{vibr}, T) + k_{nr}(\text{el}, T) \qquad (2)$$

in which $k = 1/\tau$ is the observed rate constant, k_r is the radiative rate constant, k_{nr} is the rate constant of the temperature-independent nonradiative deactivation processes, k_{nr}(vibr, T) is the rate constant of the deactivation vibrational processes, and k_{nr}(el, T) is the rate constant of the temperature-dependent electronic-based nonradiative processes. Indeed, $Eu(^5D_0)$ is sensitive to deactivation by ligand-to-metal charge transfer states (LMCT),[28,29] in particular in Eu(III) macrocyclic complexes containing nitrogen donor atoms.[30−32] Both the ligand singlet[33] and/or triplet[32] states may be deactivated in a temperature-dependent process k_{nr} (el, T). Since the $Eu(^5D_0)$ lifetime of site I in **EuL¹** is temperature-dependent contrary to the $Tb(^5D_4)$ lifetime in nonhydrated **TbL¹**, we suspect that such a de-activation mechanism may be present in **EuL¹**, although no corresponding absorption band could be located in the absorption and reflectance spectra due to potential overlap with the ligand absorptions. Assuming that the dipole strength of the magnetic dipole transition $Eu(^5D_0 \rightarrow ^7F_1)$ is independent of the Eu^{III} environment, the radiative lifetime t_r of the $Eu(^5D_0)$ level is given by eq 3:[25]

$$k_r = \frac{1}{\tau_r} = A_{MD,0} n^3 \left(\frac{I_{tot}}{I_{MD}}\right) \qquad (3)$$

in which $A_{MD,0}$ = 14.65 s^{-1} is the spontaneous emission probability of the $^5D_0 \rightarrow ^7F_1$ transition, n is the refractive index of the medium, and I_{tot}/I_{MD} is the ratio of the total emission area (J = 0−6) to the area of the $Eu(^5D_0 \rightarrow ^7F_1)$ transition. In our case, n = 1.56 (as measured at room temperature on films deposited on quartz plates), I_{tot}/I_{MD} = 5.93 (site I, 10 K) and 7.43 (site II, 10 K); therefore, $t_{r(I)}$ = 3.03 ms and $t_{r(II)}$ = 2.42 ms. The luminescence efficiency of the Eu^{III} ion is given by:[25]

$$Q_{Eu}^{Eu} = \tau_{obs}/\tau_r \qquad (4)$$

The resulting Q_{Eu}^{Eu} values are 36 and 25% at 10 and 295 K, respectively, for site I, and 21% for site II at 10 K, consistent with the efficient deactivation through the bound water molecule. The relative contributions of temperature-dependent and temperature-independent

(25) Werts, M. H. V.; Jukes, R. T. F.; Verhoeven, J. W. *Phys. Chem. Chem. Phys.* **2002**, *4*, 1542.
(26) Horrocks, W. D., Jr.; Sudnick, D. R. *J. Am. Chem. Soc.* **1979**, *101*, 334.
(27) Beeby, A.; Clarkson, I. M.; Dickins, R. S.; Faulkner, S.; Parker, D.; Royle, L.; de Sousa, A. S.; Williams, J. A. G.; Woods, M. *J. Chem. Soc., Perkin Trans. 2* **1999**, 493.
(28) Blasse, G. *Struct. Bonding* **1976**, *26*, 45.
(29) Petoud, S.; Bünzli, J.-C. G.; Glanzman, T.; Piguet, C.; Xiang, Q.; Thummel, R. P. *J. Lumin.* **1999**, *82*, 69.
(30) Ciampolini, M.; Dapporto, P.; Nardi, N. *J. Chem. Soc., Chem. Commun.* **1978**, 788.
(31) Bissell, R. A.; De Silva, A. P.; Gunaratne, H. Q. N.; Lynch, P. L. M.; Maguire, G. E. M.; Sandanayake, K. R. A. *Chem. Soc. Rev.* **1992**, 187.
(32) Sabbatini, N.; Guardigli, M.; Manet, I. In *Handbook on the Physics and Chemistry of Rare Earths*; Gschneidner, K. A., Jr., Eyring, L., Eds.; Elsevier Science: Amsterdam, 1996; Vol. 23, Chapter 154.
(33) Gonçalves e Silva, F. R.; Longo, R. L.; Malta, O. L.; Piguet, C.; Bünzli, J.-C. G. *Phys. Chem. Chem. Phys.* **2000**, *2*, 5400.

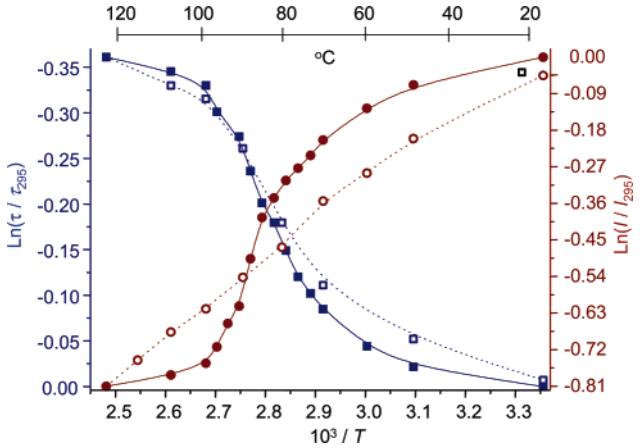

Figure 4. Integrated and corrected intensities of the Eu($^5D_0 \rightarrow {}^7F_2$) transition of **EuL¹** over its phase transition (right scale, ●: from 298 to 403 K, ○: from 403 to 298 K, excitation at 21 468 cm^{-1}); lifetimes of the Eu($^5D_0$) excited level with the analyzing wavelength set on the maximum of the $^5D_0 \rightarrow {}^7F_2$ transition (left scale, ■: from 298 to 403 K, □: from 403 to 298 K, excitation at 28 170 cm^{-1}).

processes to the deactivation of Eu($^5D_0$) in site I can now be estimated. At 10 K, temperature-dependent processes vanish,[34] so that $k_{nr} = 596\ s^{-1}$; therefore, $k_{nr}(T) = k_{nr}(\text{el.}, T) = 390\ s^{-1}$ at 295 K since OH vibrations do not contribute.

Luminescence-Detected Phase Transition. In a first series of experiments, we have measured the emission spectrum of **EuL¹** versus temperature (25−130 °C). Its intensity decreases, but its overall shape is maintained, even after the transition to the liquid crystalline state. The integrated and corrected intensities of the $^5D_0 \rightarrow {}^7F_J$ (J = 0, 2, 3 and 4) transitions, relative to the $^5D_0 \rightarrow {}^7F_1$ transition, are reported in Table S6 (Supporting Information); they do not vary within experimental error over the entire temperature range investigated, indicating that no dramatic change occurs in the nature and arrangement of the ligands in the inner coordination sphere upon the phase transition. This also means that the increased radiationless deactivation processes affect equally all the transitions to the ^7F_J levels. In subsequent experiments, we have concentrated on the most intense electric-dipole transition, $^5D_0 \rightarrow {}^7F_2$, which is known to be highly sensitive to the Eu^{III} environment,[12] accounting for about 80% of the total emission intensity. From a theoretical point of view, the temperature-dependent deactivation processes should result in an overall emission intensity (and lifetime, compare eqs 2 and 4) varying as an exponential function of the form $y = y_0 e^{-(C/RT)}$.[34,35] Therefore a graph of $\ln(I_{obs}/I_{295K})$ versus the inverse of the absolute temperature $1/T$ should be linear. This is obviously not the case in Figure 4, on which a sigmoid variation is obtained for the intensity variation of the $^5D_0 \rightarrow {}^7F_2$ emission over the transition from crystalline to liquid-crystalline phases. This sigmoid variation is not seen during the first heating cycle to 130 °C (followed by a heating stage at the latter temperature during 15 min), performed to allow for the loss of the hydration molecules. However, subsequent cycles consistently yield

(34) Kleinerman, M.; Choi Sang-Il. *J. Chem. Phys.* **1968**, *49*, 3901.
(35) Hüfner, S. *Optical Spectra of Transparent Rare Earth Compounds*; Academic Press: New York, 1978.

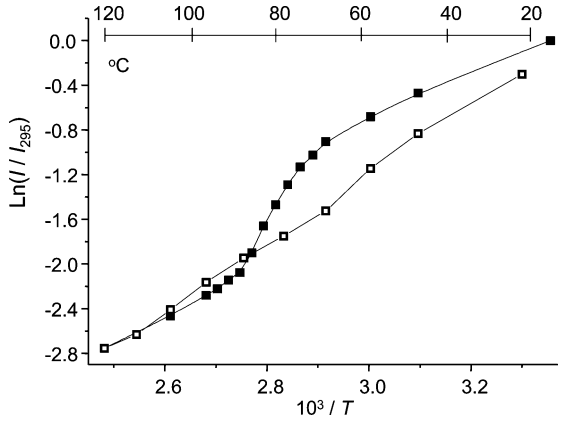

Figure 5. Integrated and corrected intensities of the Tb($^5D_4 \rightarrow {}^7F_5$) transition of **TbL¹** over its phase transition, with excitation at 20 492 cm^{-1}; ■: from 298 to 403 K; □: from 403 to 298 K.

the same starting (25 °C) and final (130 °C) values of $I(^5D_0 \rightarrow {}^7F_2)$ with the S-shaped discontinuity around the transition temperature. A mathematical analysis gives a transition temperature of 85 ± 1 °C, in very good agreement with the temperature extracted from thermal analyses (86 °C).

In addition, Figure 4 reports the variation of the Eu($^5D_0$) lifetime, which has been measured upon excitation on the Eu($^5D_2$) level while monitoring the $^5D_0 \rightarrow {}^7F_2$ transition. The corresponding graph also displays a sigmoid variation and its mathematical analysis yields a transition temperature of 83 ± 1 °C. The experiment is perfectly reproducible over several cycles (starting, as for the intensity measurements, at the second heating cycle), except for a small decrease in the high temperature (130 °C) lifetime value after 10 cycles (ca. 5%), possibly arising from a slight decomposition of the sample consecutive to the use of a high laser excitation power.

The emission intensity $I(^5D_0 \rightarrow {}^7F_2)$ displays a less marked variation upon cooling, and the analysis of the resulting curve yields 81 ± 2 °C as the transition temperature. On the other hand, the cooling curve for the lifetime retains its S-shaped aspect with a transition temperature at 86 ± 4 °C. For DSC measurements, a large hysteresis has been observed, which is a function of the cooling rate: 25 and 15 °C for rates of 5 and 0.1 °C·min^{-1}, respectively. Such an hysteresis is not seen in the luminescence experiments because the latter are recorded after the sample has been thermally equilibrated.

Since Tb^{III} is another widely used luminescence probe, we have carried out a similar study on **TbL¹**, under identical experimental conditions; here again, data have been only recorded during the second and subsequent heating/cooling cycles, the first cycle displaying features related to the loss of the solvation molecule. As a representative transition, we have chosen $^5D_4 \rightarrow {}^7F_5$ which is the most intense in the $^5D_4$ emission spectrum and quite sensitive to the metal ion environment.[12] As reported for the Eu^{III} complex, the intensity $I(^5D_4 \rightarrow {}^7F_5)$ decreases with increasing the temperature (25−130 °C, Figure 5) and the $\ln(I_{obs}/I_{295})$ versus $1/T$ curve is sigmoid with a substantial variation at the transition temperature. Its mathematical analysis gives a transition temperature of 81 ± 2 °C, identical to the one obtained

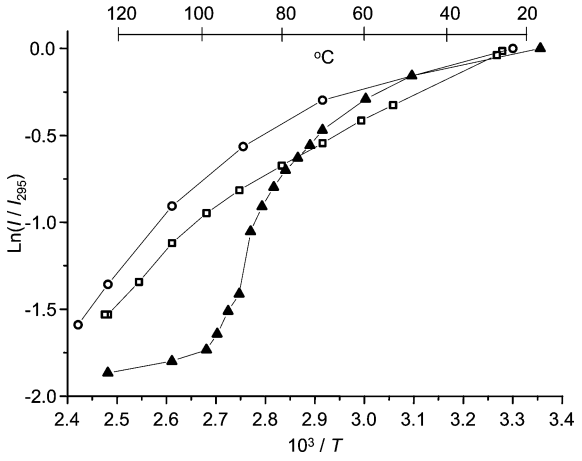

Figure 6. Integrated and corrected intensities 298 to 403 K of the Eu($^5D_0 \rightarrow {}^7F_2$) transition for **EuL¹** (▲), **EuL²** (□), and $Eu(NO_3)_3$ (○).

from thermal analysis. On the other hand, and again similarly to what has been observed for **EuL¹**, the cooling curve is almost monotonic and cannot be exploited in term of the determination of the transition temperature. This behavior is perfectly reproducible over several temperature cycles.

Origin of the Variation of the Luminescence Parameters upon Phase Transition. To further our understanding of the phenomena reported in Figure 5, we have proceeded to a detailed analysis of their origins. In a first step, we have performed the temperature-dependent measurements described above on two reference samples: anhydrous $Eu(NO_3)_3$ and **EuL²**, in which the ligand differs from **L¹** by the length of the side chain (Chart 1). The complex contains on average 1.5 water molecule by formula weight and does not display any mesogenic properties, contrary to **EuL¹**, but its emission spectrum is similar. The $\ln(I_{obs}/I_{295})$ versus $1/T$ curves for these two reference compounds are reported in Figure 6; they feature a monotonic, although not linear, dependence and are almost parallel. This variation is mainly due to the temperature-dependent nonradiative de-excitation processes (see eq 2), which must be very similar for the two compounds, particularly $k_{nr}(el, T)$, so that we have used the temperature dependence of the **EuL²** emission intensity as a corrective factor for **EuL¹**.

The **EuL¹** and **EuL²** emission intensities have been normalized at the starting temperature (25 °C), and the **EuL²** curve has then been fitted with a fourth order polynomial and its value subtracted from the **EuL¹** curve. The residual, $\ln[I(EuL^1)_{obs} - I(EuL^2)_{obs}]$, shown in Figure S7 (Supporting Information), still displays an S-shape dependence (with an inflection point around 85 °C). From a theoretical point of view, the emission intensity of a Ln^{III} ion is expressed as follows:

$$I(J, J') = \frac{64\pi^4\tilde{\nu}^3}{3h(2J+1)}\left[\frac{n(n^2+2)^2}{9} D_{ED} + D_{MD}\right] \quad (5)$$

where $I(J, J'$; in $s^{-1})$ represents the probability of spontaneous emission, $\tilde{\nu}$ is the average energy of the transition (cm^{-1}), h is Planck's constant (6.63×10^{-27} erg·s), $(2J + 1)$ is the degeneracy of the initial state (1 for Eu($^5D_0$)), while D_{ED} and D_{MD} (in $esu^2 \cdot cm^2$) are the contributions from the electric and magnetic dipole operators, respectively. Finally, n is the refractive index of the medium, which is known to undergo a nonlinear, S-shaped variation over phase transitions. Therefore, a large variation in n could be responsible for the observed changes in the luminescence intensity and lifetime on going over the phase transition. In our case, since the $^5D_0 \rightarrow {}^7F_2$ transition is purely electric dipole in nature,[36] the second term vanishes and grouping all the constants yields the simplified relationship:

$$I(0,2) = \frac{n(n^2+2)^2}{9} \times D_{ED} \times \text{cst} \quad (6)$$

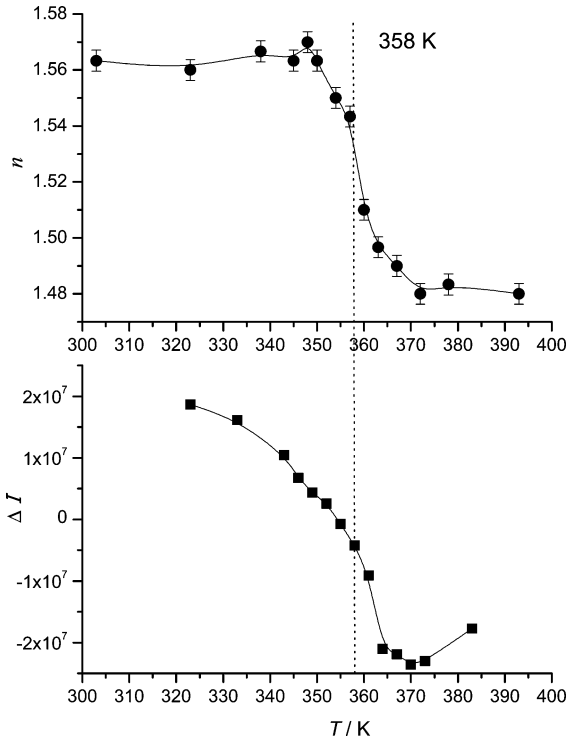

Figure 7. (Top) Refractive index of **EuL¹** (film, ●). (Bottom) Difference in emission intensity [I(**EuL¹**) − I(**EuL²**)] between 320 and 430 K, corrected for the refractive index variation using eq 6 (■).

We have consequently determined n over the 30−130 °C temperature range by measuring the reflectance spectra of a spin-coated thin film of **EuL¹** (Figure S8 in Supporting Information). Previously, we have checked that the luminescence spectrum of this film is identical to the spectrum of a finely powdered sample prepared between two Suprasil quartz plates. Moreover, before starting the measurements, the thin film has been heated at 130 °C during 15 min to eliminate water, so that measurements were perfectly reproducible over several temperature cycles. The resulting n versus $(1/T)$ curve is reported in Figure 7, together with the outcome of the division of $[I(EuL^1)_{obs} - I(EuL^2)_{obs}]$ by the $[n(n^2 + 2)^2]/9$ factor (defined as ΔI) versus $1/T$. It turns out that the correction brought by the refractive index function is relatively small and that the final $\Delta I(^5D_0 \rightarrow {}^7F_2)$ vs $1/T$ curve for **EuL¹** still presents a sharp

(36) Görller-Walrand, C.; Binnemans, K. In *Handbook on the Physics and Chemistry of Rare Earths*; Gschneidner, K. A., Jr., Eyring, L., Eds.; Elsevier Science: Amsterdam, 1998; Vol. 25, Chapter 167.

Table 3. Determination of Transition Temperature (°C) for Ln^{III} Complexes by Different Methods

compd	DSC/PLM	luminescence		refractive index
		intensity	lifetimes	
EuL¹ (heating)	86	85(1)	83(1)	86(1)
EuL¹ (cooling)		81(2)	86(4)	
TbL¹ (heating)	81	81(2)		

drop at the transition temperature, indicating that this variation is genuine to the phase transition.

The decrease in the luminescence intensity observed over the temperature range in which the mesogenic complexes **EuL¹** and **TbL¹** have been studied (25−130 °C) is attributable to several factors. An obvious one is the increased contribution of molecular vibrations and, possibly, photoinduced electron-transfer processes to radiationless de-excitation of the ^5D_J excited levels. A second one is related to the expected S-shaped decrease of the refractive index in the vicinity of the Cr→LC first-order transition (1.56 → 1.48 for **EuL¹**) which contributes about 15% to the decrease in luminescence intensity (cf. eq 6: the factor containing the refractive index varies from 3.41 to 2.89 for **EuL¹**). The remaining sigmoid variation is therefore attributable to changes intrinsic to the phase transition. A recent paper reports the luminescence properties of the nematic liquid-crystalline matrix MBBA (*N*-(4-methoxybenzylidene)-4-butylaniline) doped by Yb^{III} ion under the form of its [Yb(dbm)$_3$(phen)] complex. The authors observe a 2-fold increase of the 980-nm luminescence intensity ($^2F_{5/2}\rightarrow{}^2F_{7/2}$) in going from the isotropic phase (47 °C) to the nematic phase (12 °C) and explain this result by the fact that excitation light is scattered by the liquid-crystalline phase. The same phenomenon was also observed for a glass dispersed liquid crystal film.[37] In our case, since no change is observed in the shape and relative intensities of the $^5D_0\rightarrow{}^7F_J$ emission bands, transition to the columnar hexagonal phase does not imply a rearrangement of the inner coordination sphere of the lanthanide ions. If scattering of the excitation light by the liquid crystalline phase were the only effect operative, we should see a less pronounced temperature decrease for **LnL¹** than for the reference compounds, which is not the case, on the contrary. Therefore, an additional phenomenon occurs and we tentatively explain the residual S-shape variations of $I(^5D_0\rightarrow{}^7F_2)$, $I(^5D_4\rightarrow{}^7F_5)$ and $\tau(^5D_0)$ by an effect consecutive to the larger fluxionality of the complex molecules acquired in going from the crystalline to the less-ordered liquid-crystalline phase, generating a larger coupling between the phonon density of states and the ^5D_J electronic states.

Conclusion

This paper demonstrates that the crystalline-to-mesogenic phase transitions of **LnL¹** strongly affect the luminescence parameters of the Eu^{III} and Tb^{III} ions, thus allowing the detection of the transition temperatures. Data obtained for the latter upon monitoring luminescence parameters, namely, the $^5D_0\rightarrow{}^7F_2$ emission intensity and $^5D_0$ lifetime for Eu^{III} and the $^5D_4\rightarrow{}^7F_5$ emission intensity for Tb^{III} are compared in Table 3 with those determined by conventional methods (DSC, PLM) and by refractive index measurements. The agreement is very good, which further demonstrates the usefulness of luminescence measurements for such determinations, as recently pointed out by other authors in the case of inorganic materials and polymers.[11] In particular, luminescence intensities are easy to measure, and the data treatment is minimal, which is less the case for luminescence lifetimes.

In view of the interest presented by columnar liquid crystalline phases (e.g., for one-dimensional ion transport),[38] we are presently extending the luminescence-based investigation described here to lanthanide-containing mesogens built from bent tridentate aromatic receptors, forming both columnar and cubic phases,[4] particularly with the aim of unraveling whether an intensity jump also occurs in the case of second-order transitions.

Experimental Section

Starting Materials and General Procedures. Analytical grade solvents and chemicals (Fluka AG) were used without further purification except acetonitrile, which was distilled from CaH_2, and THF, distilled from Na and benzophenone.[39] The nitrate salts $Ln(NO_3)_3{\cdot}xH_2O$ were prepared from the corresponding oxides (Rhône-Poulenc, 99.99%) in the usual way.[40] Stock solutions of $Ln(NO_3)_3{\cdot}xH_2O$ in CH_3CN were prepared by weighting. The water content of the salt and the concentration of the solutions were determined by complexometric titrations with $Na_2(H_2EDTA)$ in the presence of urotropine and xylene orange.[41] Elemental analyses were performed by Dr. Eder, Microchemical Laboratory, University of Geneva.

Synthesis of the Ligands. *N*,*N*′-Bis{4-(3,4-di(decyloxy)-benzoyloxy)benzyl}-1,10-diaza-4,7,13,16-tetraoxacyclooctadecane (**L¹**) was synthesized as previously described,[17] while the isolation of *N*,*N*′-bis{4-(3,4-di(methoxy)benzoyloxy)benzyl}-1,-10-diaza-4,7,13,16-tetraoxacyclooctadecane (**L²**) will be detailed in a separate paper.[21]

Preparation of the Ln(III) Complexes (Ln = Eu, Tb). The Ln nitrate solution in acetonitrile or THF (10^{-1} m, 1 equiv) was added over 10 mn to a solution of **L¹** or **L²** in dichloromethane (10^{-2} M, 1 equiv). The resulting solution was stirred at room temperature during 120 min, and then the solvents evaporated. The complexes were collected as white powders by precipitation in acetonitrile (**EuL¹**, 82% yield) or by solvents evaporation (**TbL¹**, **EuL²**). Elemental analyses for $Eu(NO_3)_3L^1{\cdot}0.25H_2O$ (**EuL¹**) and $Tb(NO_3)_3L^1{\cdot}1THF$ (**TbL¹**) have been reported previously.[17] $Eu(NO_3)_3L^2{\cdot}1.5H_2O$ (**EuL²**): Calcd. for $EuC_{44}H_{54}N_5O_{21}{\cdot}1.5H_2O$ (fw: 1175.92): calcd. C, 45.2; H, 4.9; N 6.0; found: C, 45.4; H, 5.0; N, 5.8. Melting point: 159 °C.

Spectroscopic Measurements. UV−visible spectra were measured with a Lambda 900 spectrometer from Perkin-Elmer using 0.1- or 1-cm quartz cells. ^1H and ^{13}C NMR 1-D spectra were performed on a DRX-400 Bruker spectrometer, on solutions in deuterated $CDCl_3$. Low-resolution luminescence measurements (spectra and lifetimes) were recorded on Perkin-Elmer LS-50B or SPEX Fluorolog 3-22 fluorimeters. Phosphorescence lifetimes of powdered samples (quartz capillary) or solutions (1-cm Suprasil cells) were measured with the instrument in time-resolved mode. They are averages of at least three independent measurements made by monitoring the decay at the maxima of the emission spectra, enforcing a

(37) Driesen, K.; Binnemans, K. *Liq. Cryst.* **2004**, *31*, 601.

(38) Yoshio, M.; Mukai, T.; Ohno, H.; Kato, T. *J. Am. Chem. Soc.* **2004**, *126*, 994.

(39) Perrin, D. D.; Armarego, W. L. F. *Purification of Laboratory Chemicals*; Pergamon Press: Oxford, 1988.

(40) Bünzli, J.-C. G.; Moret, E.; Yersin, J.-R. *Helv. Chim. Acta* **1978**, *61*, 762.

(41) Schwarzenbach, G. *Complexometric Titrations*; Chapman & Hall: London, 1957.

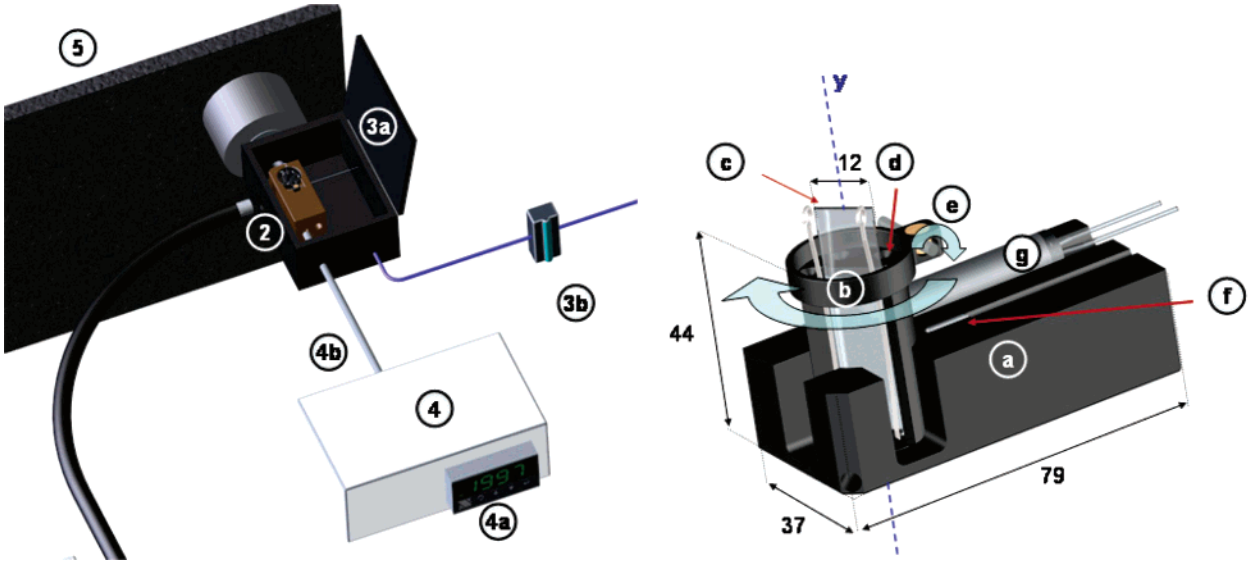

Figure 8. Schematic description of the thermostated cell holder and the thermoregulator (dimensions indicated are in mm).

0.03−0.04 ms delay. The mono- or biexponential decays were analyzed with Origin 7.0. The experimental procedures for high-resolution, laser-excited luminescence measurements has been published previously.[42] Solid-state samples were finely powdered, and low temperature (295−10 K) was achieved by means of a Cryodyne model 22 closed-cycle refrigerator from CTI Cryogenics. Luminescence spectra were corrected for the instrumental function, but not excitation spectra. Data were recorded both on powdered samples and thin films.

Characterization of the Mesophases. DSC traces were obtained either with a Setaram DSC-131 S or a Seiko DSC-220C (5−10 °C·min^{-1}, under N_2) analyzer. Thermogravimetric analyses were performed under N_2 with a Seiko TG/DTA 320 balance. Visualization of the mesophases was performed on a polarizing microscope Letiz Orthoplan-Pol with a Leitz LL 20x/0.40 polarizing objective and equipped with a Linkam THMS 600 variable-temperature unit. Preliminary small angle diffraction measurements on **EuL^1** (under N_2 atmosphere) were collected at 25, 95, and 140 °C between $2\theta = 1.4$ and 25.4° (0.03° steps) by Dr Ichiro Tobita from Rigaku Corporation X-ray Application Laboratory (Tokyo). A D/MAX Ultima II system was used (Cu Kα radiation); the sample was heated from 25 to 75 °C (10 °C/min), 95 °C (2 °C/min), 120 °C (10 °C/min), 140 °C (2 °C/min), cooled to 45 °C (10 °C/min) and 25 °C (2 °C/min), and the cycle was repeated.

Refractive Index and Thickness Measurements. The complexes were dissolved in THF (10% w/v) and the resulting solutions were dispersed onto a Suprasil quartz plate (No. 665.000-QS, 45 mm × 12.5 mm) with a Cookson Electronics P.6708 spin coater equipped with a customized vacuum chuck adapted to the quartz plate. The latter was thoroughly cleaned (Helmanex, water and ethanol) before being fitted to the vacuum chuck. The solution (20 μL) was then deposited quickly on the plate at 4000 rpm. After 10 mn spinning, its thickness (500−600 nm) was determined by an optical method. A spin-coated quartz plate was inserted onto a specially designed thermostated block (see next section). A F20 in-situ apparatus from Filmetrics was used to determine both the sample thickness and its refractive index *n*. The two optical fibers connected to the main system were held vertically above the samples, allowing collection of the light reflected from the thin film over a range of 300−1000 nm. The film thickness and its optical parameter were determined by fitting several the amplitude and periodicity of the thin film reflectance, using the software provided with the equipment. The measured and calculated spectra were compared to assess the quality of the measurements and of the fitting process.

(42) Rodriguez-Cortinas, R.; Avecilla, F.; Platas-Iglesias, C.; Imbert, D.; Bünzli, J.-C. G.; de Blas, A.; Rodriguez-Blas, T. *Inorg. Chem.* **2002**, *41*, 5336.

Luminescence Detection of Phase Transitions. The general layout of the instrumental setup is presented in Figures 8 and S9 (Supporting Information). Excitation light (no. 1) impinges on the sample fitted in a specially designed thermostated probe holder (no. 2), flushed with argon (no. 3) (to prevent sample decomposition) and controlled by a thermoregulator (no. 4). Three types of excitation light sources linked to optical fibers were used: (i) a xenon lamp coupled with a Zeiss M20 monochromator for broad-band excited emission and excitation spectra, (ii) an argon laser (465.8 and 488 nm lines) for specific excitation of the Eu($^5D_2$) or Tb($^5D_4$) levels, and (iii) a Nd:YAG laser equipped with frequency tripler (355 nm) and with an OPO crystal for lifetime measurements upon excitation of the Eu($^5D_0$) level. Light emitted by the sample was analyzed at 90° with a double monochromator (Spex Industries, 1404) (no. 5) equipped with holographic gratings. Light intensity was measured by a photomultiplier with a cooled S-20 photocathode (−20 °C, no. 6), coupled to a linear amplifier (500 MHz, no. 7) and a double photon counter (no. 8) (Standford Research Systems SR 400) for emission spectra or a SR 430 multichannel scaler from Standford Research Systems (without amplifier) for lifetime determinations. Data were transferred into a PC (no. 9) and corrected for the instrumental function. All components are connected to a controller PCI card which, in turn, transfers information to and from the computer through a program developed in the laboratory with the Labview software.

The specially designed thermostated sample holder is a blacked aluminum block (no. 2a) operating in the temperature range 20−250 °C (± 1 °C). The electronic control (no. 4) is based on a Omega CNi8 thermoregulator (no. 4a) and a HRS D-2425 Distrelec 410616 semiconductor relay (no. 4b). The argon flux (0.3 L·min^{-1}) from the 1-L reservoir (no. 3a) is controlled by a regulator (Kobold, No. KFR-2112N0; no. 3b). The rotatable circular sample holder (no. 2b) was machined out of a blackened aluminum block. The quartz plate (no. 2c) is held in position by stainless steel (No. 1.4435) clips (no. 2d). The position around the *y*-axis can be adjusted with the help of screw (no. 2e). Finally, a Pt temperature probe (no. 2f; PT 100) and the heating coil (Vulkan No. 513000, 530 Ω, length: 3.81 mm, diameter: 0.95 mm, no. 2g) are fitted into two holes with diameter 3 and 9.5 mm, respectively.

A calibration curve has been established with a 1-mm quartz cell filled with MgO and fitted with a PT-100 temperature probe in its center in order to determine the actual sample temperature (T_{meas}) as a function of the programmed temperature (T_{cons}, see Figure S10 in Supporting Information). A maximum deviation $\Delta(T_{cons} - T_{meas}) = 11.7$ °C at 240 °C is obtained, as a result of the heat dispersion in the sample box, but the correlation between the two temperature is strictly linear, with a correlation coefficient equal to 1.000. To mini-

mize the absolute error on the temperature (± 1 °C), a stabilization time of 15 min is needed before performing the measurements.

For these experiments two types of samples were used: (i) powdered samples that were deposited between two Suprasil quartz plates sealed with a Teflon film; layers of the mesogenic materials were generated by slight friction of the two plates or (ii) spin-coated samples. A typical experiment involves the following stages. Step 1: preliminary measurements at selected temperatures in order to determine the optimal excitation wavelength and the range of intensities and lifetimes spanned over the relevant temperature range. Step 2: the experimental parameters, as well as the temperature profile, are entered into the specially designed Labview software. Typical parameters are (i) initial temperature (heating rate of 1−5 °C min^{-1}); (ii) stabilization time, at least 15 min; (iii) measurement cycle time, 2−15 min; (iv) temperature intervals, typically 3 °C, 15−20 °C before and after the phase transition. Step 3: data collection and semiautomatic treatment. Step 4: repeat measurement cycle. Note that samples must been protected from contact with atmosphere.

Acknowledgment. This research is supported through grants from the Swiss National Science Foundation (National research program 47 “Supramolecular Materials”). We thank Mr. Franck Alain Nüesch (Laboratory for Optoelectronics and Molecular Materials, EPFL) for his help in determining the film thickness, Dr Ichiro Tobita from Rigaku Corporation for the X-ray analysis of **EuL^1**, Dr Jean-Pierre Rivera (University of Geneva) for polarized light microscopy analyses, and H. Lartigue (University of Geneva) for thermogravimetric analyses.

Supporting Information Available: Seven tables and 10 figures (PDF). This material is available free of charge via the Internet at http://pubs.acs.org.

CM049754T